



ZnO/Ag–Ag₂O microstructures for high-performance photocatalytic degradation of organic pollutants

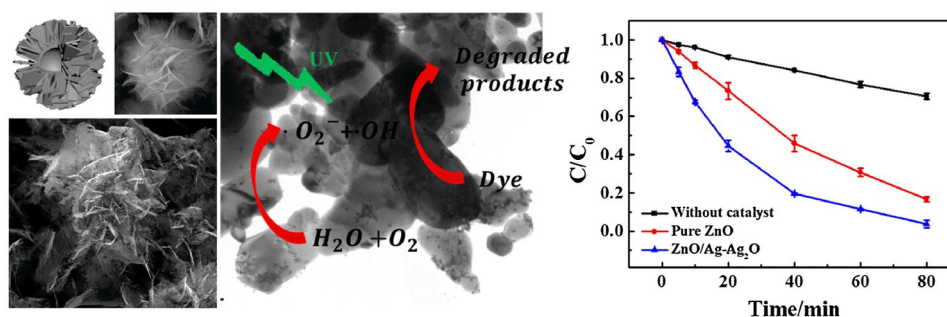
Yingchun Su¹ · Xiaole Zhao¹ · Yajun Bi¹ · Xiaojun Han¹

Received: 16 October 2017 / Accepted: 7 November 2018 / Published online: 15 November 2018
© Springer-Verlag GmbH Germany, part of Springer Nature 2018

Abstract

Organic pollutants cause serious impacts on environment. A novel method to synthesize ZnO/Ag–Ag₂O microstructures was developed for organic pollutant photocatalytic degradation. The 3D pompon-like Zn(OH)_{1.68}(SO₄)_{0.16}·0.58H₂O microspheres were firstly synthesized in a creative way by combining reaction in ethanol/water mixing layer and room-temperature self-assembly together. The length of nanosheets on Zn(OH)_{1.68}(SO₄)_{0.16}·0.58H₂O microspheres was controlled from ~0.8 to ~4.4 μm successfully. The method reduced both the processing temperature and reaction time compared with conventional ripening, which shortened catalysts' production cycle, reduced production cost and simplified production condition. It holds great potential for industrial application. As traditional nanocatalysts are not easy to recycle and the residual nanocatalysts are also potential danger to the environment, our microsized ZnO/Ag–Ag₂O photocatalysts inherit advantages of both nanoparticles and microspheres with enhanced removal efficiency and excellent recycle ability. Ag–Ag₂O nanoparticles in ZnO/Ag–Ag₂O microstructures were used to enhance the photocatalytic performance. 83.2% and 96.3% degradation efficiencies of Congo red were achieved by pure ZnO and ZnO/Ag–Ag₂O microstructures after 80 min irradiation by UV light. 78.2% and 95.6% degradation efficiencies of methylene blue were achieved by pure ZnO and ZnO/Ag–Ag₂O after 40 min under UV radiation. The degradation rate constants by ZnO/Ag–Ag₂O microstructures are 0.04056 min⁻¹ for Congo red and 0.07629 min⁻¹ for methylene blue respectively. The ZnO/Ag–Ag₂O photocatalyst showed excellent stability and reusability, since it was reused at least 5 times without any extra treatment. The ZnO/Ag–Ag₂O microstructures may hold potential for organic pollutant treatments.

Graphical abstract



Keywords 3D pompon-like ZnO · Self-assembly · ZnO/Ag–Ag₂O microstructures · Photocatalytic degradation · Congo red

Electronic supplementary material The online version of this article (<https://doi.org/10.1007/s10098-018-1641-0>) contains supplementary material, which is available to authorized users.

Extended author information available on the last page of the article

Abbreviations

SEM Scanning electron microscopy
UV Ultraviolet
XRD X-ray powder diffraction

R^2	Square linear correlation coefficients
C	Remaining concentration of organic pollutants
C_0	Initial concentration of organic pollutants

Introduction

Due to the rapid growth of economy and population, water contaminations, especially organic pollutants, have become a serious issue all over the world. Congo red is a popular benzidine-based anionic bisazo dye used in many industries. It is regarded as a typical representative of high-toxicity and hard-degradation organic pollutant in water treatment. So far, many strategies were proposed for organic pollutant treatment. Among them, the photocatalysis method has been regarded as an environmental-friendly, low-cost and sustainable process (Lee et al. 2013). During the photocatalytic process, the photocatalysts can capture photons with energy equal to or larger than their band gap energy to form electrons and holes on the surface of catalysts. It is considered that the superoxide and hydroxyl radicals are generated through the reaction between holes or electrons and water molecules to oxidize organic pollutants (Fu et al. 2015). The photocatalysts can be classified into two generic groups according to their different photocatalytic property in spectral region: ultraviolet (UV)- and visible-light-responsive photocatalysts. Many photocatalysts were reported for Congo red removal under visible-light irradiation. The chitosan/CdS (1.5 g L^{-1}) removed 85.9% of Congo red (20 mg L^{-1}) under a 300 W xenon lamp for 180 min (Zhu et al. 2009a). And 0.5 g L^{-1} of $\text{SrFe}_{12}\text{O}_{19}$ was used to remove 90% of Congo red (13.9 mg L^{-1}) under a 125 W high-pressure Hg lamp for 180 min (Mohanta et al. 2013). For $\text{Ag}_2\text{O}/\text{Ag}_2\text{CO}_3$, only 0.8 g L^{-1} of catalyst was mixed with higher concentration of Congo red (80 mg L^{-1}) under a 500 W metal halide lamp (with an ultraviolet cutoff filter) for 20 min to reach 87.5% degradation (Zhao et al. 2017). Compared with visible-light irradiation, UV irradiation showed higher Congo red degradation effect. The dye degradation of 94% (Congo red, 10 mg L^{-1}) was obtained by $\text{ZnS}-\text{Co}^{2+}$ catalysts (0.8 g L^{-1}) under UV irradiation from a 100 W low-pressure mercury-vapor lamp (Pouretedal et al. 2010). The higher degradation efficiency of 95.2% was achieved by the $\text{WO}_3-\text{TiO}_2/\text{AC}$ catalysts (10 g L^{-1}) for 40 mg L^{-1} of Congo red with a 500 W high-pressure mercury-vapor lamp illuminating for 2 h (Sun et al. 2009).

Recently, ZnO-based semiconductor photocatalysts with wide band gap, excellent chemical and physical stability and optoelectronic property have been regarded as promising materials for degrading organic dyes (Wang et al. 2018). Different approaches have been used for the preparation of ZnO, including solvothermal method (Guruvammal et al. 2016), solgel method (Ciciliati et al. 2015) and self-assembly method (Guo et al. 2015). Among them, self-assembly

approach at room temperature attracted great attention due to the low-cost and mild reaction characteristics (Sau and Murphy 2004). Various methods were employed to improve the catalytic activity of ZnO via controlling its morphology (Chen et al. 2017), doping other chemical elements (Jesudoss et al. 2016), loading noble metal particles (Zhang et al. 2010), etc. Ag (Sampaio et al. 2017) and Ag_2O (Yan et al. 2016) were reported as popular items in composite materials for ZnO photocatalysis to increase the UV-visible light adsorption intensity as well as the light adsorption range. The Ag- Ag_2O composites can be a good choice for ZnO to enhance the photocatalytic ability.

The previous photocatalysts still hold some drawbacks, such as complex synthesis process, hard recycle and low degradation rate. Most photocatalysts with strict operation condition and high manufacturing cost would block their further industrial application. A simple and green method is necessary for preparing high-efficient photocatalysts. As the normal nanoparticles are not effective for recovery from water treatment process, microsized ZnO spheres can be a better choice, and with the help of nanosized Ag- Ag_2O composites, the photocatalysts also possess special properties of nanomaterials. Most importantly, the improvement in photocatalysis performance is always the challenge for organic wastewater treatment. ZnO/Ag- Ag_2O microspheres with high-efficient photocatalytic capability can be a better choice for future industrial applications.

Herein, we successfully fabricated a novel ZnO/Ag- Ag_2O microstructure by a simple and green method as photocatalysts for Congo red degradation. The reaction at ethanol/water mixing layer was used to form $\text{Zn}(\text{OH})_{1.68}(\text{SO}_4)_{0.16} \cdot 0.58\text{H}_2\text{O}$ microspheres coated with nanosheets. The length of $\text{Zn}(\text{OH})_{1.68}(\text{SO}_4)_{0.16} \cdot 0.58\text{H}_2\text{O}$ nanosheets can be controlled by the reaction time. The combination of reaction at ethanol/water mixing layer and room-temperature Ostwald ripening was firstly developed to prepare 3D pompon-like $\text{Zn}(\text{OH})_{1.68}(\text{SO}_4)_{0.16} \cdot 0.58\text{H}_2\text{O}$ microspheres. After thermal treatment, the 3D pompon-like ZnO spheres were prepared. 3D pompon-like ZnO microspheres were decorated with Ag- Ag_2O nanoparticles through reduction in silver nitrate. Coupling with Ag- Ag_2O nanoparticles, the photocatalytic activity of 3D pompon-like ZnO microspheres for Congo red was enhanced by 13.1%. The ZnO/Ag- Ag_2O microstructures may find great application in organic pollutant treatments.

Materials and methods

Materials

Zinc sulfate monohydrate, ammonium hydroxide solution, ethanol, silver nitrate, sodium borohydride, barium sulfate

and Congo red were purchased from Sigma-Aldrich (China). All chemicals were used without any further purification. Ultrapure water (18.2 M Ω cm) was used for solution preparation in all experiments.

Preparation of 3D pompon-like ZnO spheres

The zinc sulfate monohydrate powders (0.1414 g) were mixed with 100 mL ethanol under ultrasonication for 2 h to form a crystal suspension. The diluted ammonium hydroxide solution (100 mL, 0.16 M) was dropped into the crystal suspension by violent shaking for 1 min. The white precipitations were formed immediately. The 3D pompon-like Zn(OH)_{1.68}(SO₄)_{0.16}·0.58H₂O microspheres were formed after 75 min. To make sure the reaction is complete, the reaction time was increased to 6 h. The Zn(OH)_{1.68}(SO₄)_{0.16}·0.58H₂O microspheres were washed by water and ethanol using low-speed centrifugation for three times, followed by drying in a vacuum oven at 60 °C. The 3D pompon-like Zn(OH)_{1.68}(SO₄)_{0.16}·0.58H₂O microspheres became ZnO products after heating them at 800 °C for 8 h.

Preparation of ZnO/Ag–Ag₂O nanocomposites

As-synthesized ZnO products (0.5 g) were added into 50 mL AgNO₃ solution (2.3 mM) under gentle stirring for 30 min. Then the freshly prepared NaBH₄ (0.5 mL, 0.46 M) was added into the mixture for further 6 h under stirring. The productions were washed by low-speed centrifugation for three times and dried in a vacuum oven. The ZnO/Ag–Ag₂O microstructures were formed successfully.

Adsorption ability and photocatalysis activity measurements

In adsorption experiments, 40 mg of catalysts was dispersed in 50 mL Congo red (40 mg L⁻¹) aqueous solution in a quartz tube. At certain time intervals (0, 5, 10, 20, 30 and 40 min), 3 mL of the mixture was taken out and centrifuged. The supernatant (2 mL) was measured by a UV–Vis spectrometer to calculate the concentration of Congo red in solution. The adsorption kinetic curves were then obtained. For photodegradation experiments of Congo red, 40 mg of catalysts was dispersed in 50 mL Congo red (40 mg L⁻¹) aqueous solution in a quartz tube. The above mixture was stirred for 30 min to reach the adsorption–desorption equilibrium in dark. Afterward, the suspensions were exposed to the UV-light irradiation with stirring. The irradiance value (1758–1734 W m⁻²) is tested by a radiometer FZ-A (Photoelectric Instrument Factory of Beijing Normal University, China) at the level of the photocatalytic process with 30 min preheating of mercury lamp. After different reaction times, 3 mL of suspension was extracted and centrifuged to get

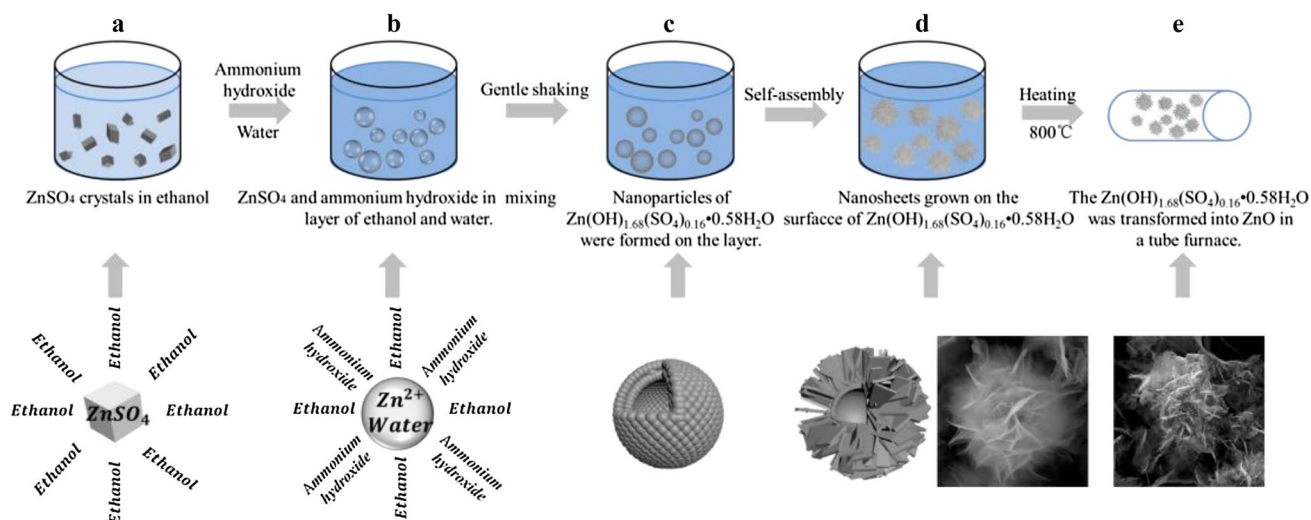
2 mL supernatant without catalysts. The 2 mL supernatant was analyzed by the UV–Vis spectrophotometer to obtain the concentrations of the remaining Congo red. After measurement, the 2 mL supernatant and the centrifuged photocatalysts were resuspended by ultrasonication and fed back into the quartz tube. For reusing experiments, 40 mg of catalysts was dispersed in 50 mL Congo red (40 mg L⁻¹) aqueous solution in a quartz tube. Under the same conditions with the above-mentioned photodegradation experiment, the solutions were irradiated under the UV light for 80 min. After irradiation, the solutions were centrifuged to recycle the catalysts. The 2 mL supernatant was extracted and analyzed by the UV–Vis spectrophotometer to obtain the concentrations of the remaining Congo red. The recycled photocatalysts were washed by water and ethanol for three times to remove extra Congo red. They were dried under vacuum oven at 60 °C overnight. The dried photocatalysts were weighed and mixed with Congo red solution with fixed concentration of catalyst to be 0.8 mg mL⁻¹. The process was carried out for five continuous cycles to estimate their stability.

Characterizations

The sample morphologies were determined by SEM (Quanta 200 FEG; Netherlands) and TEM (H-7650 Hitachi; Japan). X-ray powder diffraction (XRD) was measured in the reflection mode (Cu K α radiation) on a diffractometer (D/Max-RB, Japan) in the range of 20°–90°. UV–Vis spectra were obtained using a Cary 60 spectrophotometer (Agilent, US). The inductively coupled plasma optical emission spectroscopy (ICP-OES) was used to measure the Ag and Zn elements. The diffuse reflectance spectra were analyzed by Hitachi-4100 UV–Vis spectrophotometer (Japan) with an integrating sphere to record the diffuse reflectance spectra of the powder samples with BaSO₄ as a reference.

Results and discussion

The pompon-like Zn(OH)_{1.68}(SO₄)_{0.16}·0.58H₂O microspheres were prepared via a combination of precipitation reaction in the ethanol/water mixing reaction layer and room-temperature self-assembly as shown in Scheme 1. Through long-time ultrasonic treatment (2 h), the zinc sulfate monohydrate bulks were broken into small crystals in ethanol (Scheme 1a). Then, the diluted ammonium hydroxide solution (with water) was added and mixed with ethanol solution immediately. The zinc sulfate crystals were dissolved by water; meanwhile, the ethanol/water mixing layer containing zinc sulfate and ammonium hydroxide was formed (Scheme 1b). The two reactants in the mixing layer reacted to form the small particles of Zn(OH)_{1.68}(SO₄)_{0.16}·0.58H₂O,



Scheme 1 The schematic synthetic process for the pompon-like ZnO spheres

followed by their aggregating into microspheres (Scheme 1c). Due to the Ostwald ripening, the free nanoparticles spontaneously aggregate into 2D nanosheets on the Zn(OH)_{1.68}(SO₄)_{0.16}·0.58H₂O microspheres. The nanosheets were grown and assembled into 3D flower-like structures (Scheme 1d). By heating Zn(OH)_{1.68}(SO₄)_{0.16}·0.58H₂O microspheres at 800 °C for 8 h, the pompon-like ZnO microstructures were finally produced (Scheme 1e). It is a special non-template

method using ethanol and water mixing layer to form microstructures.

The morphologies of the Zn(OH)_{1.68}(SO₄)_{0.16}·0.58H₂O microstructures and ZnO products were investigated by SEM as shown in Fig. 1. The Zn(OH)_{1.68}(SO₄)_{0.16}·0.58H₂O (Fig. 1a, b) and ZnO (Fig. 1d, e) microspheres both showed similar 3D pompon-like structure and similar size. Their diameters are 17.5 ± 5.6 and 19.1 ± 7.3 μm, respectively. In Fig. 1b, there are many regular nanosheets grown on the

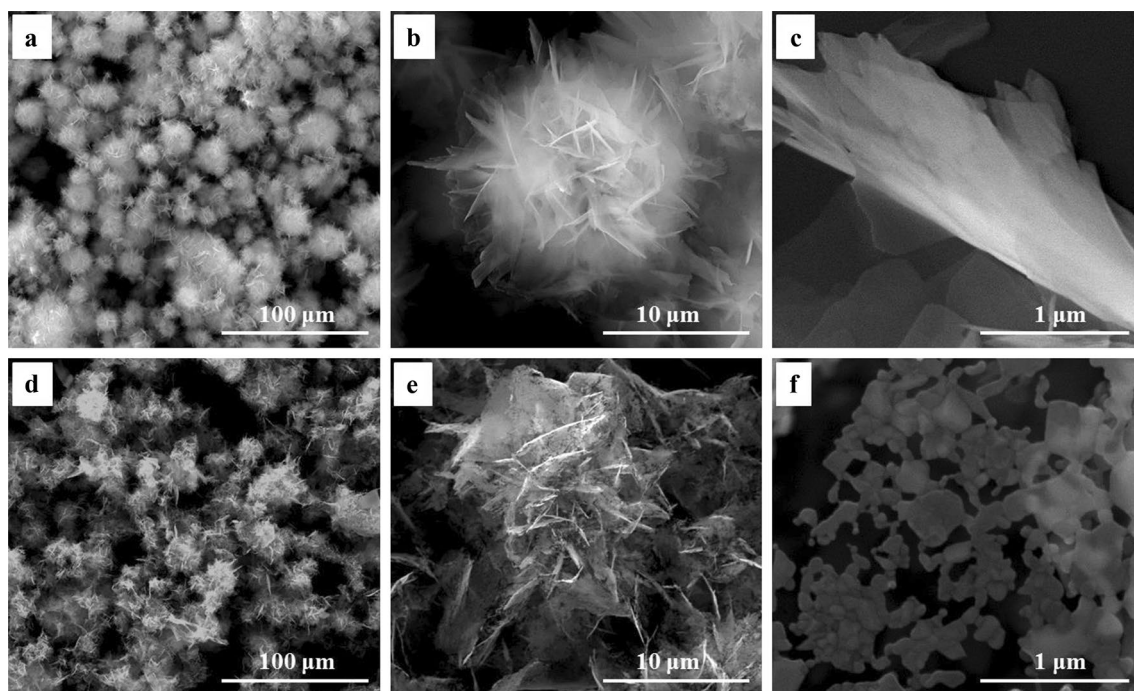


Fig. 1 SEM images of Zn(OH)_{1.68}(SO₄)_{0.16}·0.58H₂O microstructures (**a**, **b** and **c**) and ZnO products (**d**, **e** and **f**)

surface forming the special 3D pompon-like structure. The nanosheets of Zn(OH)_{1.68}(SO₄)_{0.16}·0.58H₂O microspheres (Fig. 1c) are smooth, but became porous after calcination (Fig. 1f). The thickness of Zn(OH)_{1.68}(SO₄)_{0.16}·0.58H₂O nanosheets is 2.3 ± 0.5 nm measured by AFM (Fig. S1).

The formation processes of Zn(OH)_{1.68}(SO₄)_{0.16}·0.58H₂O microstructures are shown in Fig. 2. The ZnSO₄ crystals are marked by white arrows in Fig. 2. The transformation of ZnSO₄ crystals to Zn(OH)_{1.68}(SO₄)_{0.16}·0.58H₂O hollow microstructures is clearly presented. The crystals of ZnSO₄ still exist as shown in Fig. 2a after adding the diluted ammonium hydroxide solution into the crystal ethanol suspension at 1 s because the dissolution of crystals takes time. At 8 s (Fig. 2b), the ethanol/water mixing reaction layer can be observed clearly, where the precipitation of Zn(OH)_{1.68}(SO₄)_{0.16}·0.58H₂O took place to form microshells. And the thickness of one hollow shell is about 0.99 μ m.

The thickness was marked by red line. After the ammonium hydroxide solution was added, the crystals in ethanol are dissolved and become smaller (Fig. 2a–c) and finally disappeared at 17 s (Fig. 2d), while the thickness of the shell increased to 1.49 μ m. The Zn(OH)_{1.68}(SO₄)_{0.16}·0.58H₂O hollow microstructures were successfully fabricated after 17 s using this method.

As shown in Fig. 3, the length of Zn(OH)_{1.68}(SO₄)_{0.16}·0.58H₂O nanosheets was controlled from 0.8 ± 0.4 to 4.4 ± 1.5 μ m by room-temperature Ostwald ripening. The immature nanosheets in Fig. 3a were just like wrinkles on the surface. The fully developed flower-like structure was similar to the pompon mum flower (Fig. 3b). After 75 min, the nanosheets were fully developed. The dissolution and crystallization were in dynamic balance, and consequently the length was not changed (Fig. 3e) any more. The hollow structure of Zn(OH)_{1.68}(SO₄)_{0.16}·0.58H₂O

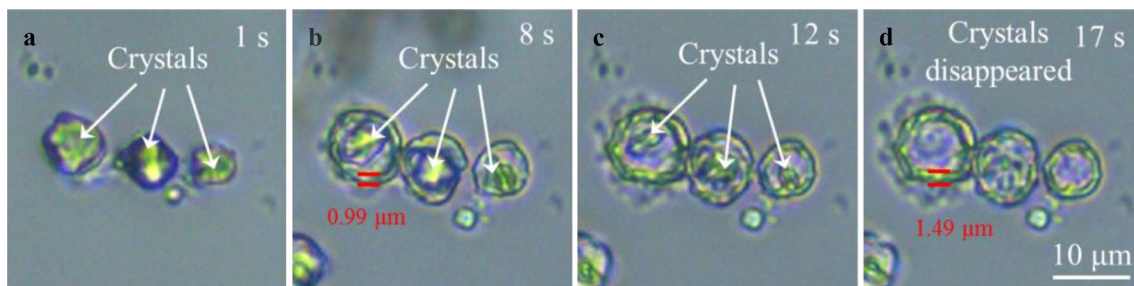


Fig. 2 The images of Zn(OH)_{1.68}(SO₄)_{0.16}·0.58H₂O microstructures formation process taken by an optical microscope. The scale bar is 10 μ m

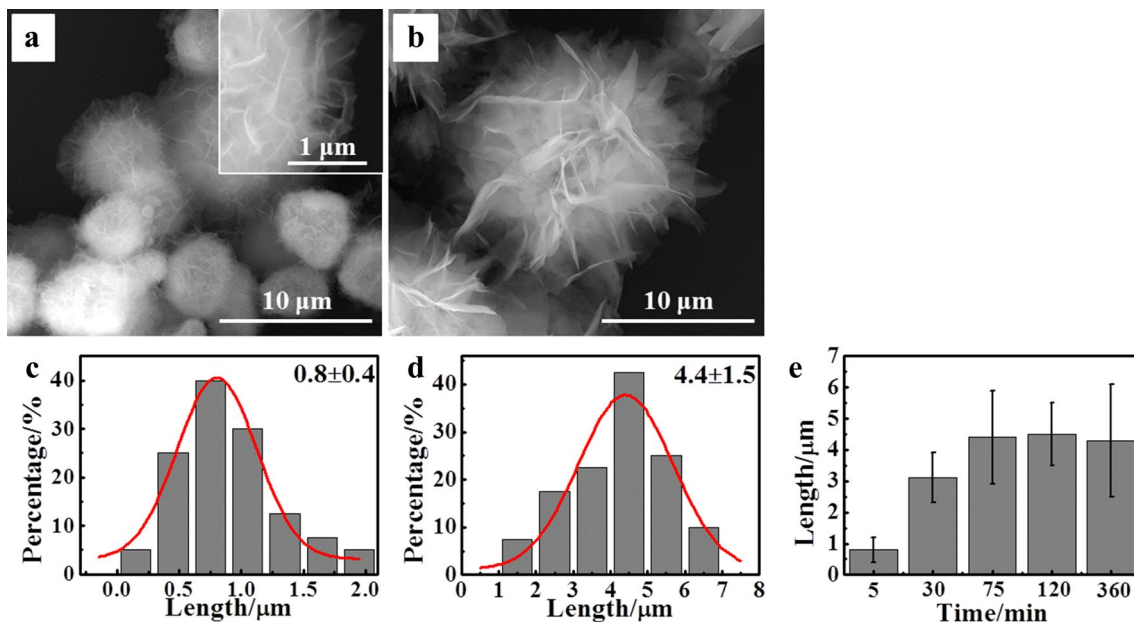


Fig. 3 The SEM images of Zn(OH)_{1.68}(SO₄)_{0.16}·0.58H₂O microspheres at different reaction times (a, 0 min and b, 75 min). c and d The length distributions of nanosheets according to SEM images. e The growth trend of nanosheets versus time

microspheres is shown in Fig. S2. The hollow structure existed at the beginning of the ripening and was kept all the time. According to previous reports, Ostwald ripening (Li and Wang 2010; Zhu et al. 2009b) needs high temperature and long time with complex solvents; however, our attractive method can be operated at room temperature, with short time and without the introduction of surfactants.

The $\text{Zn}(\text{OH})_{1.68}(\text{SO}_4)_{0.16} \cdot 0.58\text{H}_2\text{O}$ microspheres were further confirmed by element mapping based on energy-dispersive spectroscopy (EDS), where Zn, O and S are homogeneously distributed throughout the microspheres (Fig. 4a). As shown in Fig. 4b, clear and well-defined peaks of Zn, O and S can be observed in the EDS spectrum. From the EDS spectrum, the atomic fraction of microspheres can be further revealed (Fig. 4c), where the atomic ratio of Zn/O/S is 1:2.9:0.16. The possible molecular formula was proposed as $\text{Zn}(\text{OH})_{1.68}(\text{SO}_4)_{0.16} \cdot 0.58\text{H}_2\text{O}$ according to charge and matter conservation.

The TEM image (Fig. 5a) showed Ag–Ag₂O nanoparticles deposited on ZnO surfaces. The nanosized (diameter of ~ 15 nm) Ag–Ag₂O nanoparticles were homogeneously grown on the surface of ZnO. The TEM images of pure ZnO are shown in Fig. S3. It is clear that there are no nanoparticles on the surface, which confirmed that the nanoparticles on the surface are Ag–Ag₂O. In Fig. S4, the TEM of ZnO/Ag–Ag₂O microstructures after five cycling was given to show the stability. After five cycles, the Ag–Ag₂O

nanoparticles were still on the surface of ZnO, but the size and number were reduced. X-ray diffraction patterns of as-prepared samples are shown in Fig. 5b. Both ZnO sample and ZnO/Ag–Ag₂O sample had same structure with standard ZnO (PDF 79-0206). The sharp peaks in the spectra demonstrate the high crystallinity of the products. The marked peaks from the enlarged XRD spectra were originated from the structures of Ag (2θ values of 38, 44 and 64) and Ag₂O (2θ values of 33 and 38), which confirmed the particles are Ag–Ag₂O nanoparticles. The ICP-OES experiment also proved the existence of Ag element in ZnO/Ag–Ag₂O microstructures, with the ratio of Ag to Zn of 1:40. The diffuse reflectance spectra were measured to investigate the optical properties as shown in Fig. 5c, d. The absorption of ZnO is mainly less than 372 nm in the UV region and no significant absorbance can be observed in the visible light region from 400 to 800 nm. The Ag₂O was reported with a band gap of 1.2 eV and showed strong absorption of both UV and visible light (Wang et al. 2011). Ag works well between the valence band and conduction band of ZnO, which may facilitate the light absorption capacity (Karunakaran et al. 2011; Zheng et al. 2008). Hence, with Ag–Ag₂O modified on the surface of ZnO microstructures, the optical absorption of the composites can be greatly enhanced in both ultraviolet and visible light region which are related to their excellent photocatalytic activity. With the help of Ag–Ag₂O nanoparticles and also the surface roughness increase, the absorption

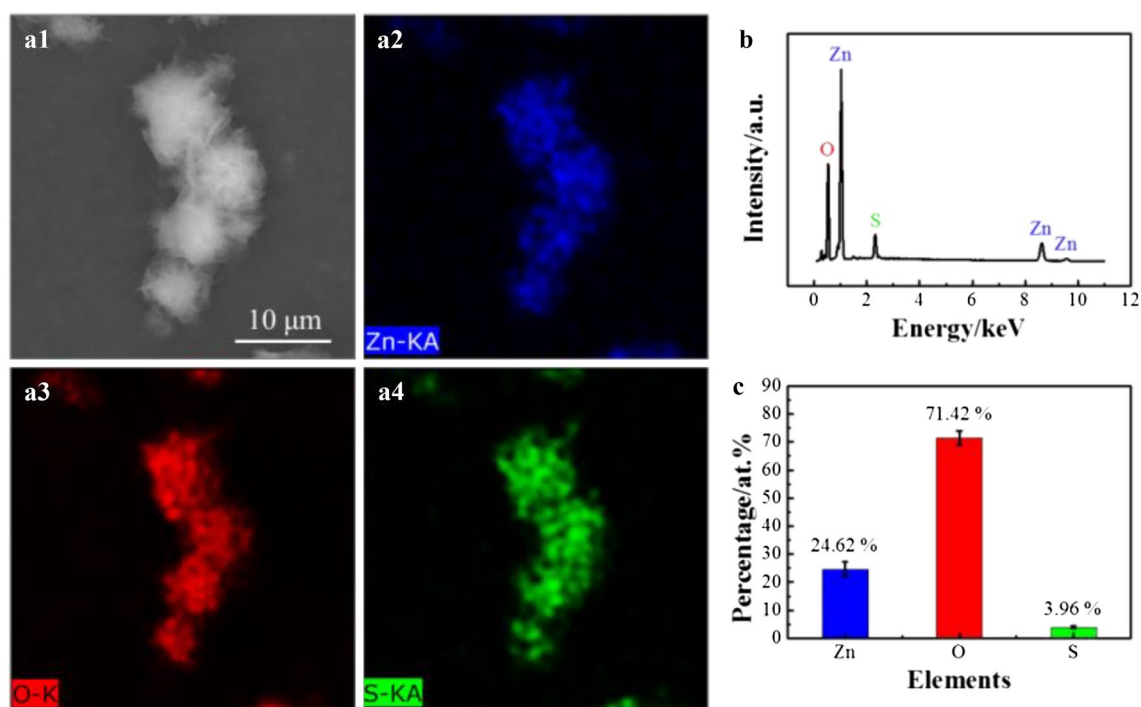
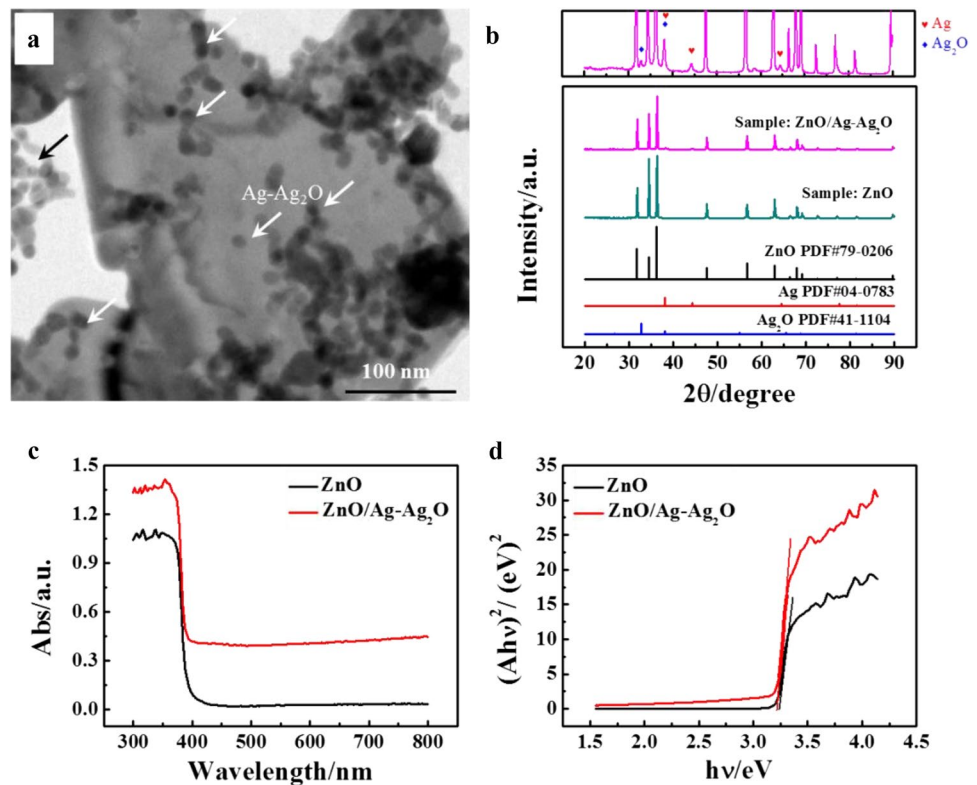


Fig. 4 The SEM image (a1), element mapping (a2, Zn element distribution; a3, O element distribution; a4, S element distribution), EDS spectrum (b) and element analysis (c) of $\text{Zn}(\text{OH})_{1.68}(\text{SO}_4)_{0.16} \cdot 0.58\text{H}_2\text{O}$ microspheres with reaction time of 75 min

Fig. 5 The TEM images of ZnO/Ag–Ag₂O microstructures (a) and their XRD patterns (b). The image on the top of b is the enlarged XRD pattern in the dotted box for ZnO/Ag–Ag₂O. UV–Vis diffuse reflectance spectra (c) and the corresponding plots to estimate the band gap values (d) of ZnO and ZnO/Ag–Ag₂O microstructures by Kubelka–Munk equation



intensity of ZnO/Ag–Ag₂O microstructures increased from 1.07 to 1.36. The roughness was measured by AFM and analyzed by Gwyddion software. By adding Ag–Ag₂O nanoparticles, the value of Ra increased from 37.91 ± 2.54 to 71.19 ± 16.45 nm, and AFM images are shown in Fig. S5. The optical band gaps of ZnO and ZnO/Ag–Ag₂O microstructures calculated by the Kubelka–Munk method were obtained to be 3.22 and 3.21 eV, respectively, as shown in Fig. 5d. It can be seen that the optical band gap of the ZnO microstructures slightly decreased by adding Ag–Ag₂O nanoparticles, which was mainly due to the quantum size effects (Xue et al. 2008).

The adsorption and photocatalytic performances of ZnO/Ag–Ag₂O microstructures under UV-light regions were investigated by degrading Congo red and methylene blue. Photodegradability-related curves are shown in Figs. 6 and 7. Figure 6a shows the adsorption capacity of pure ZnO and ZnO/Ag–Ag₂O toward Congo red at room temperature. It can be seen that the adsorption is very fast at the beginning stage, and then it becomes slower and finally reaches equilibrium after 30 min. The maximum adsorption capacity is 15.7 and 31.5 mg g⁻¹ for ZnO and ZnO/Ag–Ag₂O, respectively. The adsorption kinetic curves according to the pseudo-second-order kinetic rate model (Eq. 1) are shown in Fig. 6b, where the pseudo-second-order rate constants were 0.02963 and 0.01356 g (min mg)⁻¹ for ZnO and ZnO/Ag–Ag₂O, respectively.

$$t/q_t = 1/kq_e^2 + t/q_e \quad (1)$$

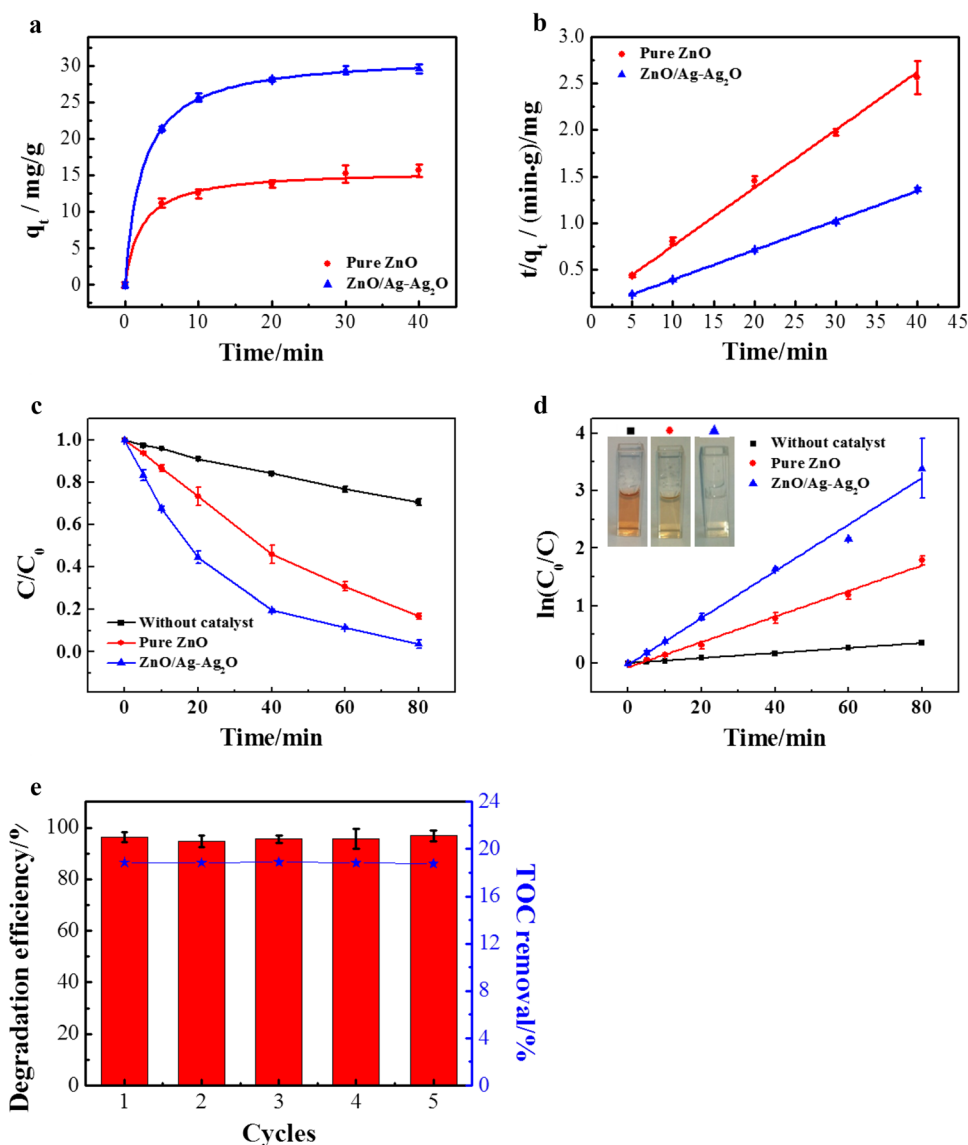
where k is the rate constant and q_t (mg g⁻¹) and q_e (mg g⁻¹) are the amount of dye sorbed at time t (min) and equilibrium state, respectively.

Due to adsorption process, 31.4% and 63.0% of total Congo red are removed for ZnO and ZnO/Ag–Ag₂O, respectively. With the help of Ag–Ag₂O composites, the adsorption ability increased. It can be explained by the effect of electrostatic adsorption shown in Fig. 7a, b. The ZnO/Ag–Ag₂O (20.1 mV) held more positive charges than ZnO (13.2 mV); thus, the negatively charged Congo red are more liable to be adsorbed on ZnO/Ag–Ag₂O. To study the photocatalysis degradation, the adsorption effect should be limited. At first, the system was conducted to equilibrium without illumination and adsorption–desorption equilibrium was reached after 30 min. After adsorption–desorption equilibrium, the removal of Congo red is mainly due to photocatalysis degradation. The characteristic peaks of Congo red at 496 nm decreased gradually without shifting and almost disappeared after 80 min irradiation. The degradation efficiency is calculated by Eq. 2:

$$\text{Degradation efficiency (\%)} = \frac{C_0 - C}{C_0} \times 100\% \quad (2)$$

where C is the concentration of the centrifuged solution after irradiation time t and C_0 is the initial concentration of the organic pollution solution.

Fig. 6 **a** Adsorption kinetics of pure ZnO and ZnO/Ag–Ag₂O for Congo red; **b** the pseudo-second-order plot transformed from curve in (a); **c** photocatalytic degradation of Congo red with no photocatalysts (black curve), ZnO microspheres (red curve) and ZnO/Ag–Ag₂O microstructures (blue curve). **d** The $\ln(C_0/C)$ against time curves derived from (c); the insets are the images of Congo red solution after 80 min irradiation under different conditions. **e** The stability test of ZnO/Ag–Ag₂O microstructures for Congo red



According to photocatalytic degradation curves in Fig. 6c, 83.2% and 96.3% degradation efficiency of Congo red were achieved by pure ZnO and ZnO/Ag–Ag₂O after 80 min. The Ag–Ag₂O composites and the increasing roughness of microstructures are the main factors to enhance degradation efficiency. The blank sample without catalysts showed only 29.5% degradation efficiency. The total organic carbon elimination efficiency of Congo red is shown in Fig. S6. 18.7% of 40 mg L⁻¹ Congo red was thoroughly degraded into CO₂ and H₂O. The kinetic curve (Fig. 6d) was fitted using the pseudo-first-order kinetics equation, $\ln \frac{C_0}{C} = kt$ where k was the first-order rate constant (min⁻¹). The calculated k value and the square linear correlation coefficients (R^2) are listed in Table 1. The k results clearly demonstrated that the ZnO/Ag–Ag₂O microstructures had the better degradation rate constant of 0.04056 min⁻¹, which is nearly twice as that of pure ZnO (0.02208 min⁻¹). The stability of the catalyst

was tested by five successive cycles for the degradation of Congo red under UV light, as shown in Fig. 6e. Degrading efficiency of five cycles were 96.3%, 94.8%, 95.6%, 95.7% and 96.8%, respectively, which confirmed excellent reusability of ZnO/Ag–Ag₂O catalysts. The photocatalytic mineralization was presented through TOC removal. Only about 18.9% of total Congo red was completely removed in the five cycles. The performances of other photocatalysts for Congo red are listed in Table 2. It is noted that our catalyst displayed higher removal efficiency than other catalysts. The ZnO/Ag–Ag₂O microstructures displayed great potential for Congo red photodegradation.

The degradation experiments for methylene blue were also presented in a similar way. The adsorption capacity of pure ZnO and ZnO/Ag–Ag₂O toward methylene blue at room temperature is shown in Fig. 7a. Only 0.13 and 0.20 mg g⁻¹ of methylene blue were adsorbed by ZnO and

Fig. 7 **a** Adsorption kinetics of pure ZnO and ZnO/Ag–Ag₂O for methylene blue; the inset is a schematic diagram to explain the difference on the adsorption (electrostatic adsorption) for Congo red (CR) and methylene blue (MB); **b** the values of zeta potential for water control, ZnO and ZnO/Ag–Ag₂O; **c** photocatalytic degradation of methylene blue with no photocatalysts (black curve), ZnO microspheres (red curve) and ZnO/Ag–Ag₂O microstructures (blue curve). **d** The $\ln(C_0/C)$ against time curves derived from (c). **e** The stability test of ZnO/Ag–Ag₂O microstructures for methylene blue (decolorization efficiency and TOC removal). **f** Photocatalytic degradation of tetracycline with no photocatalysts (black curve) and ZnO/Ag–Ag₂O microstructures (blue curve)

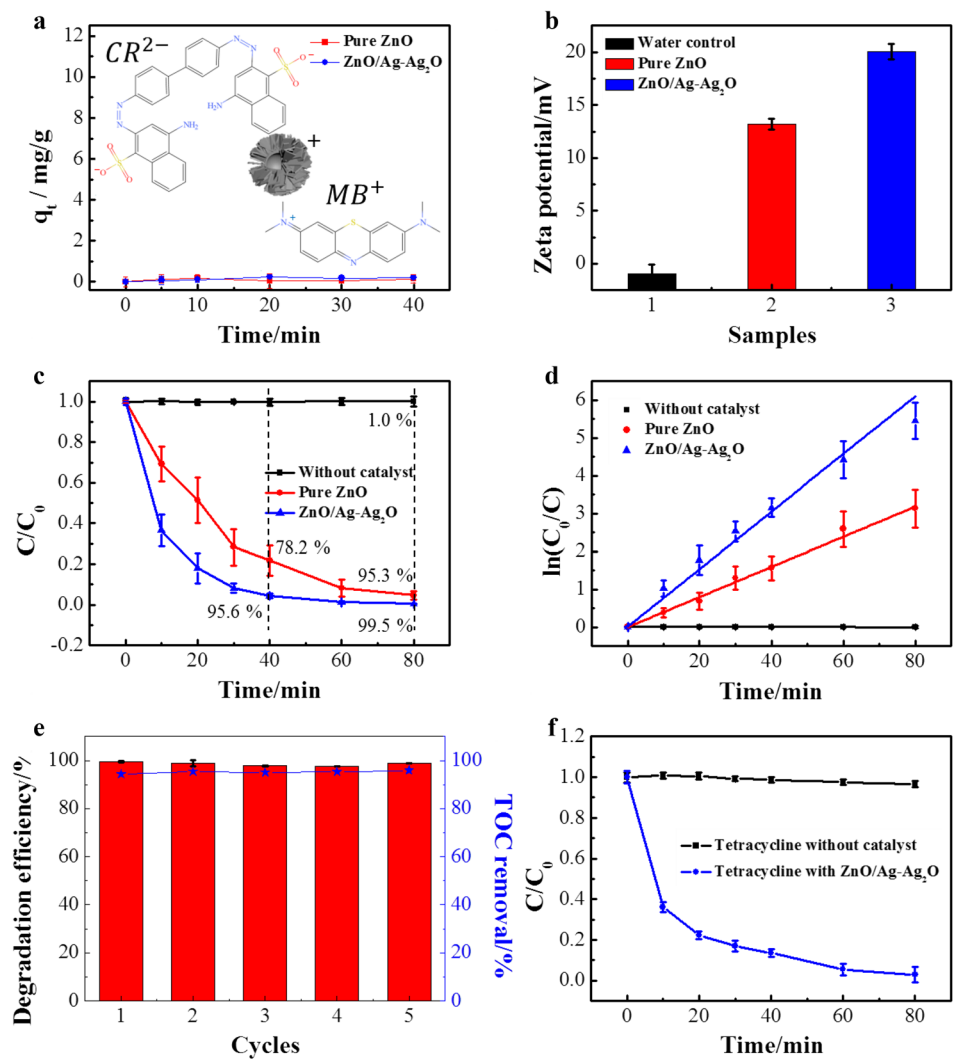


Table 1 Pseudo-first-order kinetic constant (k) and square of correlation coefficient (R^2) for photocatalytic degradation of Congo red under UV irradiation

	Blank	ZnO	ZnO/Ag–Ag ₂ O
k (min^{-1})	0.00437	0.02208	0.04056
R^2	0.9992	0.9894	0.9878

ZnO/Ag–Ag₂O after 40 min. Compared with Congo red, the catalysts showed a poor adsorption capacity for methylene blue, which can be explained by the zeta potential properties of ZnO and ZnO/Ag–Ag₂O. The zeta potential of water control, ZnO and ZnO/Ag–Ag₂O are shown in Fig. 7b. The water samples were conducted (-0.99 ± 0.92 mV) as a control group to make sure the accuracy. The ZnO and ZnO/

Table 2 Summary of reported photocatalysts for Congo red

Material	Catalyst (g L^{-1})	Time (min)	Congo red (mg L^{-1})	Degradation (%)	k (min^{-1})	Light	References
ZnO/Ag–Ag ₂ O	0.8	80	40	96.3	0.041	UV	Our work
WO ₃ –TiO ₂ /AC	10	120	40	95.2	0.026	UV	Sun et al. (2009)
ZnS–Co ²⁺	0.8	120	10	94	0.022	UV	Pouretedal et al. (2010)
Chitosan/CdS	1.5	180	20	85.9	0.011	Visible light	Zhu et al. (2009a)
Ag ₂ O/Ag ₂ CO ₃	0.8	20	80	87.5	0.068	Visible light	Zhao et al. (2017)
SrFe ₁₂ O ₁₉	0.5	180	13.9	90	–	Visible light	Mohanta et al. (2013)

Ag–Ag₂O are positively charged due to their zeta potential of 13.2 mV and 20.1 mV, respectively, where the Ag–Ag₂O nanoparticles contribute to the positive shift. The ZnO and ZnO/Ag–Ag₂O catalysts are available to adsorb the negatively charged dye, while the methylene blue holds positive charges and Congo red has negative charges according to the molecular formula in the insets of Fig. 7a. The photocatalytic degradation curves are shown in Fig. 7c. 78.2% and 95.6% degradation efficiency of methylene blue were achieved by pure ZnO and ZnO/Ag–Ag₂O after 40 min. Finally, degradation efficiency with pure ZnO and ZnO/Ag–Ag₂O was 95.3% and 99.5% at 80 min, respectively, while the blank sample without catalysts showed only 1.0% degradation efficiency. The kinetic curves (Fig. 7d) were fitted using the pseudo-first-order kinetics equation, where the calculated *k* values and *R*² coefficients are listed in Table 3. The *k* and degradation efficiency clearly demonstrated that the ZnO/Ag–Ag₂O microstructures had the better degradation ability than that of pure ZnO. The reusability of ZnO/Ag–Ag₂O catalysts for methylene blue was shown by the recycling experiment in Fig. 7e. The removal efficiency of the dyes with five cycles was all more than 97.5% and the removal efficiency of total organic carbon was nearly 95.1%, which confirmed excellent catalytic stability. Compared with other photocatalysts as shown in Table 4, ZnO/Ag–Ag₂O microstructures show excellent degradation in both decolorization efficiency and TOC removal. The ZnO/Ag–Ag₂O microstructures exhibited great potential for methylene blue photodegradation. Tetracycline was also chosen as the degradation target with an initial concentration of 10 mg L⁻¹. The suspension is irradiated under UV light for 80 min after stirring for 30 min

in a dark environment. The results are shown in Fig. 7f. The photodegradation efficiency of tetracycline is 97.1% after 80 min irradiation. These results clearly demonstrated that ZnO/Ag–Ag₂O microstructures can be used as an efficient photocatalyst for the organic wastewater treatment.

Under UV irradiation, both Ag₂O and ZnO can be simultaneously excited to form electron–hole pairs. Due to the different band gap energy (Wu et al. 2012; Ma et al. 2014), the photogenerated electrons transferred from ZnO to Ag₂O, while holes diffused from Ag₂O to ZnO. With Ag doping, the electrons in Ag₂O can arrive at the interface easily for the short mean free paths and help the charge separation (Xue et al. 2008; Umukoro et al. 2016). Due to the fast charge-transfer effect of Ag (Zheng et al. 2007), the photogenerated electrons will store on the surface of Ag nanoparticles producing superoxide oxygen radical ($\cdot\text{O}_2^-$), as shown in Fig. 8. Meanwhile the holes on the ZnO reacted with water to form

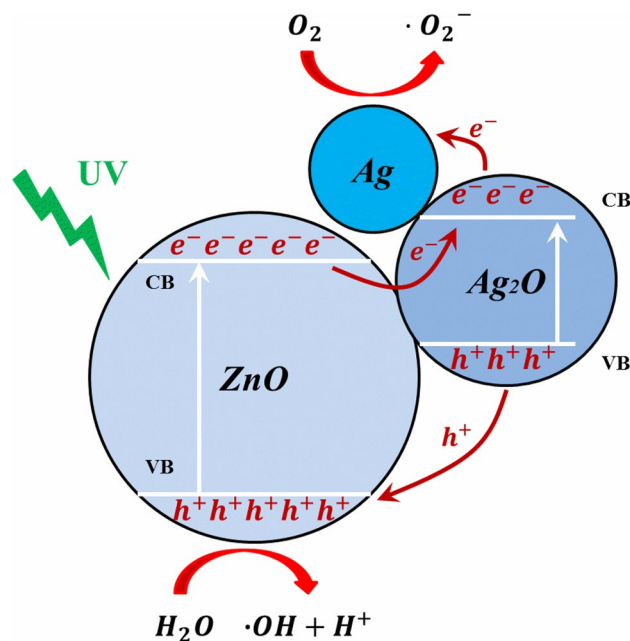


Fig. 8 Schematic of proposed photocatalytic mechanism of ZnO/Ag–Ag₂O catalyst under UV irradiation

Table 3 Pseudo-first-order kinetic constant (*k*) and square of correlation coefficient (*R*²) for photocatalytic degradation of methylene blue under UV irradiation

	Blank	ZnO	ZnO/Ag–Ag ₂ O
<i>k</i> (min ⁻¹)	0	0.03979	0.07629
<i>R</i> ²	–	0.9943	0.9883

Table 4 Summary of reported photocatalysts for methylene blue

Material	Catalyst (g L ⁻¹)	Time (min)	Methylene blue (mg L ⁻¹)	Color removal (%)	TOC removal (%)	Light	References
ZnO/Ag–Ag ₂ O	0.8	80	10	97.5	95.1	UV	Our work
Pt/WO ₃ –GO	0.5	–	3.20	94 (70 min)	92 (360 min)	Visible light	Ismail et al. (2018)
31% Fe-ACFT(PS-A20)	0.1	120	6.40–16.00	96–98	91	UV	Kadirova et al. (2017)
ZnO:Eu(1%)-M	1	–	–	90 (150 min, 10 mg L ⁻¹)	33.6 (90 min, 50 mg L ⁻¹)	Simulates solar radiation	Trandafilovic et al. (2017)
HT-DS/TiO ₂ /Fe23	0.3	120	24	96	61	UV-Vis	Miranda et al. (2015)

hydroxyl radical ($\cdot\text{OH}$) (Zhao et al. 2017; Gu et al. 2009). These radicals are the oxidants to decompose the organic dyes (Liu et al. 2013; Konstantinou and Albanis 2004).

Conclusions

ZnO/Ag–Ag₂O microstructures were synthesized for Congo red photocatalytic degradation. It is the first time that the Zn(OH)_{1.68}(SO₄)_{0.16}·0.58H₂O microspheres were fabricated by combining dynamic dissolving/precipitation reaction in ethanol/water mixing layer and particle self-assembly. The ripening of Zn(OH)_{1.68}(SO₄)_{0.16}·0.58H₂O microspheres happened at room temperature and within shorter time period compared with conventional ripening process. Although the ZnO microspheres can be used to degrade Congo red directly, the addition of Ag–Ag₂O nanoparticles enables double reaction rate and enhanced the degradation efficiency by 13.1% from 83.2 and 96.3%. Compared with previously reported ZnO/Ag photocatalysts (Guy and Ozacar 2016) with 81.6% removal for Congo red, our result enhanced degradation efficiency by 14.7%. The ZnO/Ag–Ag₂O microstructures hold great potential for organic pollutant photodegradation with high removal efficiency.

Acknowledgements This work was supported by the National Key R&D Program of China (2016YFC0401104), HIT Environment and Ecology Innovation Special Funds (HSCJ201617), the National Natural Science Foundation of China (Grant Nos. 21773050, 21528501), and State Key Laboratory of Urban Water Resource and Environment (Harbin Institute of Technology) (No. 2017DX05).

Compliance with ethical standards


Conflict of interest The authors declare that they have no conflict of interest.

References

- Chen H, Zhao L, Wang GH, He X, Wang XT, Fang W, Du X (2017) Direct growth of ZnO nanorods on biogenic hierarchical rice husk SiO₂ and their application to dye degradation. *Clean Technol Environ* 19:1335–1345
- Ciciliati MA, Silva MF, Fernandes DM, de Melo MAC, Hechenleitner AAW, Pineda EAG (2015) Fe-doped ZnO nanoparticles: synthesis by a modified sol–gel method and characterization. *Mater Lett* 159:84–86
- Fu YS, Huang T, Zhang LL, Zhu JW, Wang X (2015) Ag/g–C₃N₄ catalyst with superior catalytic performance for the degradation of dyes: a borohydride-generated superoxide radical approach. *Nanoscale* 7:13723–13733
- Gu CD, Cheng C, Huang HY, Wong TL, Wang N, Zhang TY (2009) Growth and photocatalytic activity of dendrite-like ZnO@Ag heterostructure nanocrystals. *Cryst Growth Design* 9:3278–3285
- Guo SY, Zhao TJ, Jin ZQ, Wan XM, Wang PG, Shang J, Han S (2015) Self-assembly synthesis of precious-metal-free 3D ZnO nano-
- micro spheres with excellent photocatalytic hydrogen production from solar water splitting. *J Power Sources* 293:17–22
- Guruvammal D, Selvaraj S, Sundar SM (2016) Effect of Ni-doping on the structural, optical and magnetic properties of ZnO nanoparticles by solvothermal method. *J Alloys Compd* 682:850–855
- Guy N, Ozacar M (2016) The influence of noble metals on photocatalytic activity of ZnO for Congo red degradation. *Int J Hydrogen Energy* 41:20100–20112
- Ismail AA, Faisal M, Al-Haddad A (2018) Mesoporous WO₃-graphene photocatalyst for photocatalytic degradation of methylene blue dye under visible light illumination. *J Environ Sci China* 66:328–337
- Jesudoss SK, Vijaya JJ, Selvam NCS, Kombaiiah K, Sivachidambaram M, Adinaveen T, Kennedy LJ (2016) Effects of Ba doping on structural, morphological, optical, and photocatalytic properties of self-assembled ZnO nanospheres. *Clean Technol Environ* 18:729–741
- Kadirova ZC, Hojamberdiev M, Katsumata KI, Isobe T, Matsushita N, Nakajima A, Okada K (2017) Fe₂O₃-loaded activated carbon fiber/polymer materials and their photocatalytic activity for methylene blue mineralization by combined heterogeneous-homogeneous photocatalytic processes. *Appl Surf Sci* 402:444–455
- Karunakaran C, Rajeswari V, Gomathisankar P (2011) Enhanced photocatalytic and antibacterial activities of sol–gel synthesized ZnO and Ag–ZnO. *Mat Sci Semicond Proc* 14:133–138
- Konstantinou IK, Albanis TA (2004) TiO₂-assisted photocatalytic degradation of azo dyes in aqueous solution: kinetic and mechanistic investigations—a review. *Appl Catal B Environ* 49:1–14
- Lee SS, Bai HW, Liu ZY, Sun DD (2013) Novel-structured electrospun TiO₂/CuO composite nanofibers for high efficient photocatalytic cogeneration of clean water and energy from dye wastewater. *Water Res* 47:4059–4073
- Li BX, Wang YF (2010) Facile synthesis and enhanced photocatalytic performance of flower-like ZnO hierarchical microstructures. *J Phys Chem C* 114:890–896
- Liu SY, Cai Y, Cai XY, Li H, Zhang F, Mu QY, Wang YJ, Wang YD (2013) Catalytic photodegradation of Congo red in aqueous solution by Ln(OH)₃ (Ln = Nd, Sm, Eu, Gd, Tb, and Dy) nanorods. *Appl Catal A General* 453:45–53
- Ma SS, Xue JJ, Zhou YM, Zhang ZW (2014) Photochemical synthesis of ZnO/Ag₂O heterostructures with enhanced ultraviolet and visible photocatalytic activity. *J Mater Chem A* 2:7272–7280
- Miranda LDL, Bellato CR, Milagres JL, Moura LG, Munteer AH, de Almeida MF (2015) Hydrotalcite-TiO₂ magnetic iron oxide intercalated with the anionic surfactant dodecylsulfate in the photocatalytic degradation of methylene blue dye. *J Environ Manag* 156:225–235
- Mohanta O, Singhababu YN, Giri SK, Dadhich D, Das NN, Sahu RK (2013) Degradation of Congo red pollutants using microwave derived SrFe₁₂O₁₉: an efficient magnetic photocatalyst under visible light. *J Alloys Compd* 564:78–83
- Pouretedal HR, Beigy H, Keshavarz MH (2010) Bleaching of Congo red in the presence of ZnS nanoparticles, with dopant of Co²⁺ ion, as photocatalyst under UV and sunlight irradiations. *Environ Technol* 31:1183–1190
- Sampaio MJ, Lima MJ, Baptista DL, Silva AMT, Silva CG, Faria JL (2017) Ag-loaded ZnO materials for photocatalytic water treatment. *Chem Eng J* 318:95–102
- Sau TK, Murphy CJ (2004) Room temperature, high-yield synthesis of multiple shapes of gold nanoparticles in aqueous solution. *J Am Chem Soc* 126:8648–8649
- Sun JH, Wang YK, Sun RX, Dong SY (2009) Photodegradation of azo dye Congo Red from aqueous solution by the WO₃-TiO₂/activated carbon (AC) photocatalyst under the UV irradiation. *Mater Chem Phys* 115:303–308
- Trandafilovic LV, Jovanovic DJ, Zhang X, Ptasincka S, Dramicanin MD (2017) Enhanced photocatalytic degradation of methylene

- blue and methyl orange by ZnO: Eu nanoparticles. *Appl Catal B Environ* 203:740–752
- Umukoro EH, Peleyeju MG, Ngila JC, Arotiba OA (2016) Photocatalytic degradation of acid blue 74 in water using Ag–Ag₂O–ZnO nanostructures anchored on graphene oxide. *Solid State Sci* 51:66–73
- Wang XF, Li SF, Yu HG, Yu JG, Liu SW (2011) Ag₂O as a new visible-light photocatalyst: self-stability and high photocatalytic activity. *Chem Eur J* 17:7777–7780
- Wang H, Liang LF, Cheng XJ, Luo YM, Sun S (2018) Facile fabrication of porous ZnS and ZnO films by coaxial electrospinning for highly efficient photodegradation of organic dyes. *Photochem Photobiol* 94:17–26
- Wu M, Yan JM, Zhao M, Jiang Q (2012) Facile synthesis of an Ag₂O–ZnO nanohybrid and its high photocatalytic activity. *ChemPlusChem* 77:931–935
- Xue H, Xu XL, Chen Y, Zhang GH, Ma SY (2008) Influence of Ag-doping on the optical properties of ZnO films. *Appl Surf Sci* 255:1806–1810
- Yan F, Liu Y, Cai X, Wu X (2016) Facile synthesis of Ag₂O nanoparticles decorated ZnO assemblies with excellent photocatalytic performances. *J Nanosci Nanotechnol* 16:8538–8543
- Zhang YA, Xu JQ, Xu PC, Zhu YH, Chen XD, Yu WJ (2010) Decoration of ZnO nanowires with Pt nanoparticles and their improved gas sensing and photocatalytic performance. *Nanotechnology*:21
- Zhao XL, Su YC, Qi XD, Han XJ (2017) A facile method to prepare novel Ag₂O/Ag₂CO₃ three-dimensional hollow hierarchical structures and their water purification function. *ACS Sustain Chem Eng* 5:6148–6158
- Zheng YH, Zheng LR, Zhan YY, Lin XY, Zheng Q, Wei KM (2007) Ag/ZnO heterostructure nanocrystals: synthesis, characterization, and photocatalysis. *Inorg Chem* 46:6980–6986
- Zheng YH, Chen CQ, Zhan YY, Lin XY, Zheng Q, Wei KM, Zhu JF (2008) Photocatalytic activity of Ag/ZnO heterostructure nanocatalyst: correlation between structure and property. *J Phys Chem C* 112:10773–10777
- Zhu HY, Jiang R, Xiao L, Chang YH, Guan YJ, Li XD, Zeng GM (2009a) Photocatalytic decolorization and degradation of Congo Red on innovative crosslinked chitosan/nano-CdS composite catalyst under visible light irradiation. *J Hazard Mater* 169:933–940
- Zhu LP, Liao GH, Yang Y, Xiao HM, Wang JF, Fu SY (2009b) Self-assembled 3D flower-like hierarchical beta-Ni(OH)₂ hollow architectures and their in situ thermal conversion to NiO. *Nanoscale Res Lett* 4:550–557

Affiliations

Yingchun Su¹ · Xiaole Zhao¹ · Yajun Bi¹ · Xiaojun Han¹ 

✉ Xiaojun Han
hanxiaojun@hit.edu.cn

¹ State Key Laboratory of Urban Water Resources and Environment, School of Chemistry and Chemical Engineering, Harbin Institute of Technology, 92 West Da-Zhi Street, Harbin 150001, China